Semi-automated crater depth measurements

Sylvain Breton, Cathy Quantin-Nataf, Thomas Bodin, Damien Loizeau, Matthieu Volat, Loic Lozac'h

MethodsX 6 (2019) 2293–2304

Contents lists available at ScienceDirect

MethodsX

journal homepage: www.elsevier.com/locate/mex

Method Article

Semi-automated crater depth measurements

Sylvain Breton*, Cathy Quantin-Nataf, Thomas Bodin, Damien Loizeau, Matthieu Volat, Loic Lozac'h

Université Lyon 1, France

A B S T R A C T

Impact cratering is a major process driving planetary landscape evolution. Statistics of craters spatial density is extensively used to date planetary surfaces. Their degradation state and morphometry are also key parameters to understand surface processes.

To exploit the increasing coverage of digital terrain models (DEM) on Mars at high spatial resolution, we propose a semi-automated pipeline for crater depth measurement based on coupled optical images and DEM. From a craters map shapefile coupled with a co-registered DEM, we propose to measure crater depth as the difference between the 60th percentile of elevation values on the edge of the crater and the 3rd percentile value of the elevations within the crater. We present here this method and its calibration.

- Aside to this paper, we provide a simple python code of this pipeline.
- This method can rapidly produce crater depth dataset big enough to be interpreted statistically.
- We provide solid tests on the precision of measured crater depth. Especially, we show that minimal elevation value within a crater, sometime used as crater floor elevation, is a far less precise approximation than a low percentile of elevation.

A R T I C L E I N F O

Method name: Semi-automated crater depth measurements

Keywords: Mars, Surface, Cratering, Image processing

Article history: Received 20 May 2019; Accepted 7 August 2019; Available online 23 August 2019

* Corresponding author.

E-mail addresses: sylvain.breton@univ-lorraine.fr (S. Breton), cathy.quantin-nataf@univ-lyon1.fr (C. Quantin-Nataf), thomas.bodin@ens-lyon.fr (T. Bodin), icdamien@gmail.com (D. Loizeau), matthieu.volat@univ-lyon1.fr (M. Volat).

https://doi.org/10.1016/j.mex.2019.08.007

Specifications Table

Subject Area:	Earth and Planetary Sciences
More specific subject area:	Crater morphometry
Method name:	Semi-Automated Crater Depth Measurements
Resource availability:	Python code in the supplementary material

Background

Impact craters are observed on every solid body of the solar system and drive the landscape evolution on many planetary surfaces. Their number, spatial density and shape hold key clues to planetary landscapes evolution [1–4].

The most common use of impact craters statistics is the analysis of their size-frequency distribution to study the exposure age of a planetary surface to meteoritic bombardment [5–7]. Thanks to the Apollo sample-return missions, a correlation has been established between the crater size-frequency distribution of lunar geological units and ages provided by radiometric dating [7,8]. Since then, we can attribute an absolute model age to planetary surfaces based on their crater size-frequency distribution [8]. However, the number of craters visible on a planetary surface can be affected by other parameters. Several studies investigated how crater size-frequency distributions were affected by phenomena such as resurfacing events by surfaces processes [9–12] or how the presence of a thick atmosphere modified the number of small craters [13]. Investigating these processes requires more complex models and thus complementary observations of crater shapes and densities.

Craters morphometry analysis is widely used, as parameters describing the shape and geometry of craters are affected by a wide range of phenomena [14,3,15,16]. First, the shape of the craters depends on impact dynamics. In cases of strength-dominated impacts, craters feature simple bowl-shape while in cases of gravity-dominated impacts, complex craters with a central peak are observed [3]. The target properties also play a role in the initial crater shape [14,17–19].

The observed shape of an impact crater not only depends on its formation conditions but also on its evolution. A wide range of surface processes affects the morphometry of craters. Among those processes, we can include sedimentary cycles (e.g. [12,20]), lava flows and degradation by new craters (e.g. [21,22]). Analyzing crater modification from their pristine shape is a way to probe the geological history of the crater vicinity.

Observation of degradation states of craters demonstrate that Noachian craters were highly degraded while Hesperian craters were less modified and Amazonian craters were rarely modified (e.g. [20,23]). To quantify crater degradation processes, the ratio between the crater depth and its diameter is widely used [14,24–31]. Assuming the initial depth of a crater, its observed depth to diameter ratio depends on age and obliteration rate, as the crater is filled by deposits and the rims are eroded [32].

Studies of Martian craters morphometry have already been conducted. Some provide scaling laws between depth and diameter for fresh craters ([33] and therein), while other focus on crater degradation with time [32,34,35]. However, those studies often rely on a restricted number of craters or mainly focus on large craters. Robbins and Hynek [27] database provide crater depth for Martian craters with a diameter larger than 3 km. With the growth of high-resolution imagery, below 10 m/pixel, it becomes now possible to study the dynamics and degradation of small impact craters on Mars (smaller than 100 m). In this diameter range, target properties may affect the initial crater/depth ratio [3,14,28]. This diameter range also covers many secondary craters which are generally shallower than primaries [26,36]. The increasing coverage of Martian surface by the Context Camera (CTX) images from The Mars Reconnaissance Orbiter mission (MRO) makes it possible to massively compute digital terrain models (DEM) using stereo-photogrammetry. Thousands of CTX DEMs are now available or computable for analyzing Martian small craters morphometry [37].

In their review of crater depth measurements, Robbins et al. [33] recommend avoiding unsupervised depth determination algorithms. For instance, automatic craters mapping programs detect circular depressions on DEM and give depth measurements [28], but those methods miss the shallowest craters. On the other hand, manual extraction of individual crater morphometry is time-consuming. Semi-automated depth measurements seem to be a good compromise between the two approaches.

Here we present a semi-automatic algorithm for measuring crater depths on a DEM. Crater depths are measured as the difference between the high 60^{th} percentile value of elevations on the edge of the crater and the low 3^{rd} percentile value of elevations within the crater. We describe the algorithm and the used imagery, which allows to rapidly produce large datasets of crater depth. We calibrated the parameters of the method by comparing produced depths with measurements made at higher spatial resolution. This comparison also provides error estimates on our measured depth. Quantification of the error allows a more robust exploitation of crater statistics with the kernel density estimation, providing continuous depth or diameter distributions.

Imagery datasets and processing

Mars surface elevation is described by various elevation datasets. First, a global model was produced by Mars Orbital Laser Altimeter (MOLA) onboard Mars Global Surveyor (MGS). Elevations from MOLA have been converted into a global DEM with a spatial resolution (*Rs*) of 463 m/pixel [38]. Other Martian DEMs are produced by stereo-photogrammetry, from two images taken from different observation angles, and are aligned on MOLA data.

Mainly three instruments are used to perform stereo-photogrammetry on Mars. The High Resolution Stereo Camera (HRSC) onboard Mars Express (*Rs* = 12–25 m/pixel) [39,40], CTX onboard MRO (*Rs* = 6 m/pixel) [41,42] and HiRISE (High Resolution Imaging Science Experiment) also onboard MRO mission (*Rs* = 50 or 25 cm/pixel) [43,44].

The increasing coverage of Mars by visible imagery allows creating DEMs by stereo-photogrammetry with a better spatial resolution than MOLA. The calculated DEMs have at best the spatial resolution of the used images. The vertical resolution (*Rv*) of the DEM is not precisely determined but is expected to be around $^1/_4$ of the horizontal resolution of the images used for the stereo-photogrammetry [45]. The use of CTX and HiRISE stereo-photogrammetry data has been recommended to study crater morphometry, even for large craters, as the precision of these data is better than Mars Orbiter Laser Altimeter (MOLA) data [46].

All the management of images: images download, calibration, map-projection, DEM and ortho-images calculation have been performed thanks to the MarsSI application. The MarsSI application uses the AMES stereo-pipeline [45] to produce CTX or HiRISE DEMs and associated ortho-images on demand [37]. MarsSI produces DEMs with generic parameters, this allows easier and faster production of DEMs. However, computed products may contain more noise than a manually calibrated DEM. In order to quantify the coverages, we computed global coverages of the various data-set using MarsSI footprints.

Despite being the highest spatial resolution, HiRISE data suffers very low spatial coverage (~4% of image coverage and ~0.3% of stereo-coverage). CTX images offer a very good trade-off between coverage and resolution with a resolution allowing to assess the morphometry of craters down to 50 m of diameter and a coverage large enough to provide sufficient crater statistics (almost 100% of image coverage and ~17% of stereo-coverage). To better explore the ever larger CTX dataset, we propose a semi-automated depth measurements workflow, with a manual crater mapping a CTX image and an automatic rim to floor depth extraction from an aligned DEM.

In order to design and calibrate our automatic measurements and assess the precision of our depth measurements, we performed manual crater rim to floor depth measurements using HiRISE DTMs and orthoimages, as this data-set has a higher spatial resolution and precision than CTX data set.

Description of the semi-automatic pipeline

Manual crater mapping on CTX images

The fact that Ames stereo-pipeline provides a DEM perfectly aligned with an ortho-image is crucial. Visible imagery allows precise and rapid mapping of craters, even of the most degraded ones. With a crater map aligned with the DEM, it is possible to extract elevation information within and around the crater in order to measure depth.

We perform crater mapping on the CTX ortho-images under GIS environment (QGIS). Each crater is represented by a circle manually drawn from 2 points on opposite sides of the rim and stored as a polygon shapefile. Fig. 1 illustrates the mapping approach. This method may not be the most precise as it introduces an error on non-circular craters and craters with degraded rims [47]. However, the mapping is rapid and similar to the one proposed by the CraterTools extension of ArcGIS, a widely used tool in planetary science [48].

Description of the automatic pipeline

We provide aside this paper a code written in python. From a craters map saved as a shapefile and an associated DEM in the same projection system, this program computes depth for each crater and adds it, as a new attribute, to the shapefile. This section describes the algorithm used to measure depth.

The elevation of the floor of the crater can simply be estimated by the minimum elevation within the crater. However, DEMs may contain artifacts both of natural origin (subsequent craters on the floor) or artificial origin (DEM computation errors). To better assess the deepest point of the initial crater, we choose to use a low percentile. For each crater, we extract the elevation values of each pixel within the circle. Those elevation values are weighted by the area of the surface of the pixel included within the circle. From these elevations and weights, we compute a histogram and extract percentiles values (Fig. 1C).

The rim elevation is more difficult to estimate. Indeed, the rim can be unequally degraded, by surface processes and/or affected by younger impact craters. In order to consider this bias, we not only compute the median elevation value of the pixels touching the edge of the crater, but also higher percentiles value of those values. The provided code computes crater depth as the difference between the 60^{th} percentile of elevation values on the edge of the crater and the 3^{rd} percentile value of the elevations within the crater according the tests we present in the following section.

Parametrization

Creation of the test dataset

In order to design and calibrate our automatic measurements and assess the precision of our depth measurements, we performed manual crater rim to floor depth measurements using HiRISE DTMs and orthoimages, as this data-set has a higher spatial resolution than CTX data set. Our calibration set is composed of 182 craters depth measurements at HiRISE scale where HiRISE and CTX DEM were overlapping. Table 1 lists the used images. Fig. 2 is a histogram of diameters and depth of the test sample, the size frequency distribution follows a power law, which is representative of a classic crater database [49].

Crater depth can be either defined as the difference between the local surface and the bottom of the crater elevations or as the difference between the rim and the crater bottom elevations ([33] and references therein). We exclude the first method as the local surface is never homogenous in impacted surfaces, which may lead to large error in the measurements. We focus here on rim to floor depth. To perform such a measurement, a precise map of the rim is required, excluding local anomalies caused, for example, by other subsequent craters on the rim.

We manually mapped the floor and the rim of the crater on HiRISE images. The lowest point of the crater floor has been mapped as a polygon using HiRISE DEMs and images. The rim has been mapped

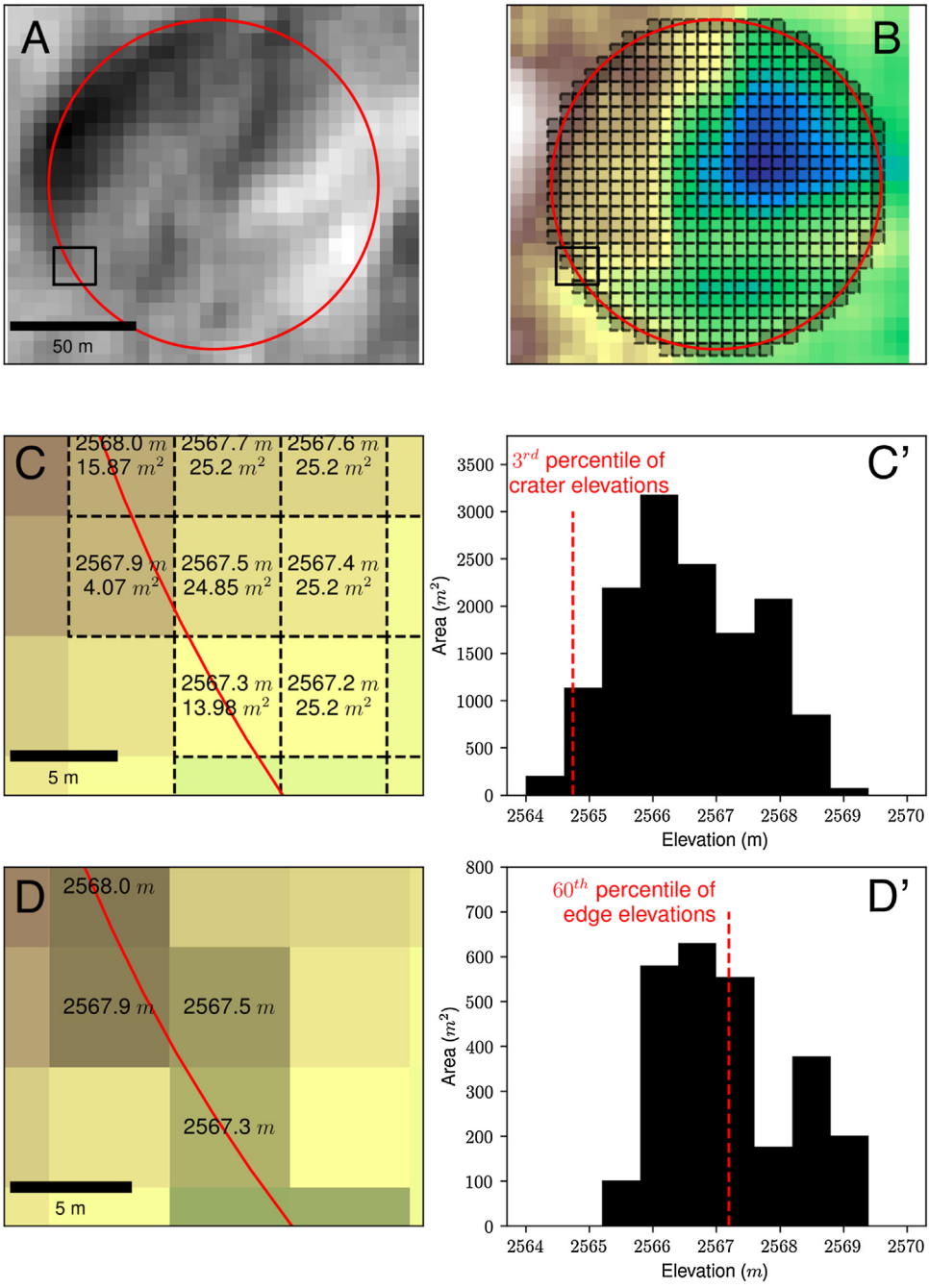

Fig. 1. The crater (red circle) is mapped on a CTX stereo-image (A). Depth is measured from the associated CTX DEM (B). (C) and (D) are close-ups on the crater edge. (C) illustrates how the pixels elevation values are weighted according to the intersecting area with the crater resulting in a weighted histogram (C'). (D) illustrates how the pixels representing the rim are selected, from those pixel values, the 60th percentile of elevation is computed (D').

Table 1
list of the used images for the test set.

Site ID	HiRISE orthoimages	DEM source	CTX orthoimages MarsSI and AMES	Number of craters
1	PSP_001782_1655 PSP_002204_1655	AMES stereo-pipeline	P02_001782_1657_XI_14S321W P03_002204_1657_XI_14S321W	10
2	ESP_011365_1365 ESP_011642_1365	HiRISE DEM Team	B04_011365_1364_XN_43S239W B05_011642_1364_XN_43S239W	19
3	ESP_017417_1655 ESP_016916_1655	AMES stereo-pipeline	B19_016916_1654_XN_14S230W B20_017417_1657_XN_14S230W	48
4	ESP_013213_1705 ESP_013635_1705	AMES stereo-pipeline	J04_046377_1728_XN_07S296W J05_046588_1709_XN_09S296W	34
5	ESP_024222_1590 ESP_024723_1590	AMES stereo-pipeline	G15_024222_1590_XN_21S252W G17_024723_1590_XN_21S253W	34
6	ESP_019346_1690 ESP_020190_1690	HiRISE DEM Team	G05_020190_1689_XN_11S334W G03_019346_1689_XN_11S334W	5
7	ESP_025174_1660 ESP_028207_1660 and ESP_028629_1660 ESP_029051_1660	AMES stereo-pipeline	G18_025174_1656_XN_14S325W D05_029051_1659_XN_14S325W	10
7'	ESP_029908_1660 ESP_029974_1660 and ESP_028629_1660 ESP_029051_1660	AMES stereo-pipeline	D05_029051_1659_XN_14S325W D07_029908_1662_XN_13S325W	22

as a polyline using HiRISE image excluding the parts of the rim degraded by other craters. We applied a 1 m buffer around the rim polyline (Fig. 3). Floor and rim elevation were then extracted as the median elevations of respectively the floor polygon and the rim buffer, using the raster statistic tool of QGIS.

These depth measurements at HiRISE scale are used to calibrate the parameters of the algorithm used to measure the depth on CTX data. We do not consider HiRISE measurements as foolproof, but we

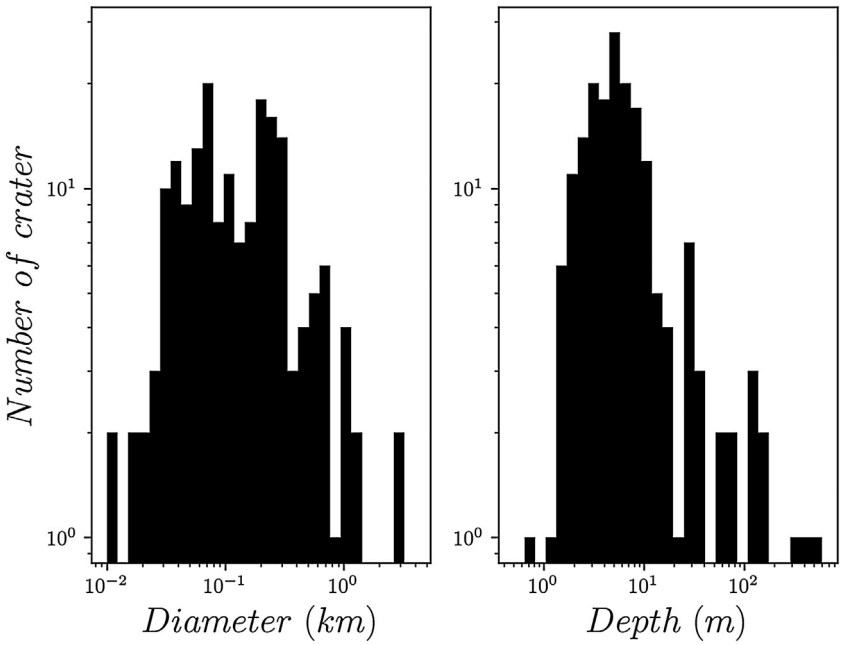

Fig. 2. Histogram of the diameters and depths of the test dataset. Both distributions are logarithmic. Our test sample presents depth and diameter distribution similar to observed crater populations.

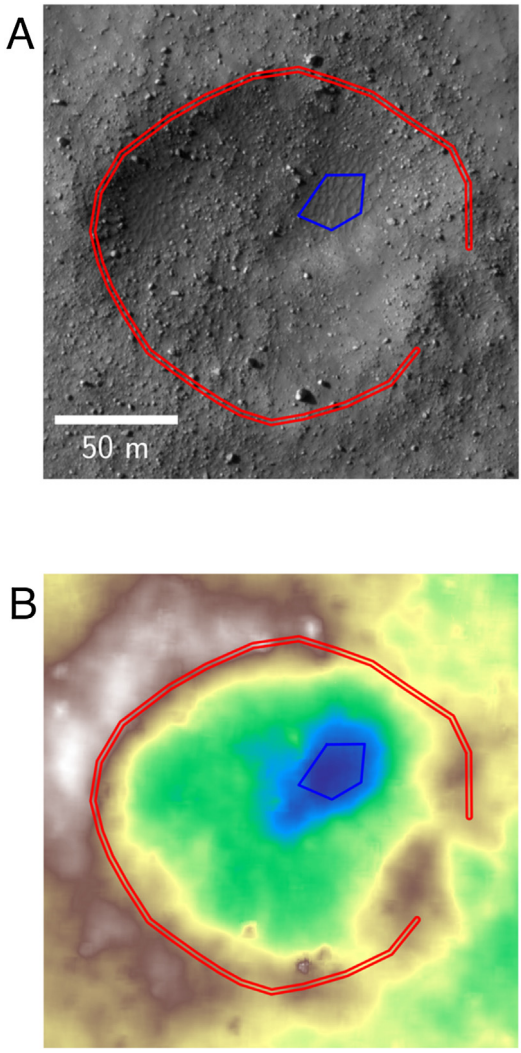

Fig. 3. Crater rim (red) and floor (blue) mapping on HiRISE stereo-image (A) and elevation map from HiRISE DEM (B). Crater represented is the same than in Fig. 1.

estimated that their error is negligible compared to CTX measurements. The next section describes how we used this test dataset to find the best floor and the rim elevation estimations.

Parameter tests

For a crater *i*, we note $\boldsymbol{d}_{a,i}$, the depth measured by our algorithm on CTX dataset and $\boldsymbol{d}_{m,i}$, the precise data measured on HiRISE (we consider the error on this measurement to be negligible). We note $\boldsymbol{r}_i = \boldsymbol{d}_{a,i} - \boldsymbol{d}_{m,i}$ the residual error and $\boldsymbol{R}$ the set of the *182* residual errors.

We computed the sum of the absolute values of residual error $\chi = \sum_i |\boldsymbol{r}_i|$ to test the different percentile values. The lowest sum of residual error will determine the best percentile to use. We computed χ using different estimations of floor elevation and rim elevation. Fig. 4 represents the result of this computation for various combination of tested rim and floor elevations.

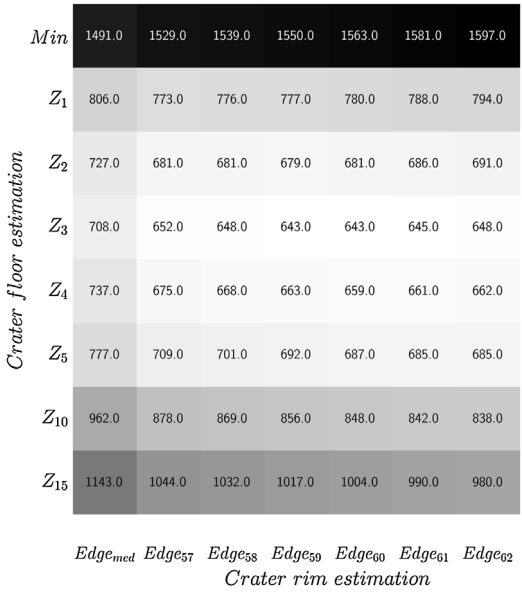

Fig. 4. Sum of residual errors represented relative to the different parameters used to estimate floor elevation and rim elevation. Z_i refers to i^{th} percentile of elevations within the crater and $Edge_i$ refers to the i^{th} percentile of elevations on the crater edge. Residual errors are both written and represented as a color. The lowest residual error corresponds to the 60^{th} percentile of elevation values of pixel touching the crater edge minus the third percentile of elevation within the crater. For clarity reasons, only the parameters around the best estimation are represented.

As shown in Fig. 4, the floor elevation estimated as the 3^{rd} percentile of elevation value within the crater, and the rim elevation as the 60^{th} percentile of elevation values on the circle edge are the measurements minimizing the error. We set these parameters of our python code, but they can be easily tuned. Fig. 4 shows that simply taking the median of elevation around the crater and the minimum elevation within the crater results in large residual error. Especially, crater floor elevation should not be approximated by the minimal elevation within the crater. Using a low percentile value provide better results for a slightly higher computation time. The minimum elevation is probably too sensitive to DEM artifacts and local elevation anomalies like smaller craters on the floor. Fig. 5 shows a

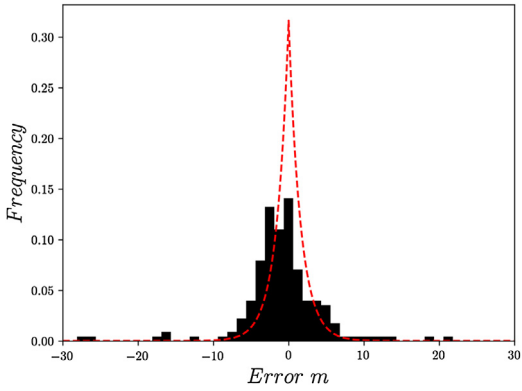

Fig. 5. Histogram of the residual error between depth computed by our program and precise HiRISE depth measurements. Red curve is the best fit with a Laplacian distribution, with a standard deviation of 5 m.

histogram of the residual error. This histogram can be described by a Laplacian law with a standard deviation of 5 m. This standard deviation seems independent from diameter or depth.

Discussion

Sources of error

We have estimated the error of our measurements to be about 5 m. This error can originate from the CTX DEM resolution. Indeed, automatically computed DEM may contain artifacts or holes, especially in area where it is difficult to correlate the stereo pairs. For instance, craters filled with sand have very smooth floors. On such smooth surfaces, correlation is challenging resulting in noisy or incomplete DEM. In such cases, the estimation of the bottom elevation of the crater may be challenging.

On the other hand, errors can also come from the approximations we made in our pipeline. For example, estimating the rim by a circle may be an issue in case of dissymmetric craters, such as the one resulting from low angle impacts, like in the case of secondary craters fields [36]. Along with this problem, we can cite the differences in diameter found by various mappers [47]. This error is estimated around 10% of the diameter of the crater. However, we expect our method to be stable regarding those variations, as the disk representing the crater has a high probability to contain both the bottom of the crater and a part of the rim. Only highly degraded craters may be a source of error as their rim can be unequally degraded.

Finally, overlapping craters can produce errors, either by increasing depth if they are within the measured crater, or by decreasing depth when located on the rim of the measured crater.

Interpretation of measured depths

This method allows the extraction of an extended crater morphometry dataset. However, the error on the measure is quite important for shallow craters. Considering a maximum depth over diameter ratio of 0.2 ([33] and therein), most craters less than 100 m of diameter are expected to have a depth less than 5 m. We recommend not to use this pipeline to measure depth for crater smaller than 100 m on CTX image. We also recommend not to use depth measured with this algorithm to interpret single crater depth as the error from a single crater depth measure may be large while on a wider data-set, the results can be statistically significant.

This algorithm is, indeed, designed to compute depth statistics for a large number of craters, typically a crater set of several hundred craters like the ones used for crater-based chronology. Depth measurements would actually add a new dimension to crater statistics. By analogy to crater size-frequency distributions, we propose the use of crater diameter vs depth frequency distributions. Those two-dimension distributions, can be used to determine, along with the age of the surface, the resurfacing history.

Conclusion

We present an algorithm that returns crater depth values from a crater map shapefile and an aligned DEM. We designed this algorithm to better interpret CTX digital terrain models (DEM). From a manually mapped crater shapefile and an aligned DEM we compute the depth as the difference between the 3^{rd} percentile of elevation value within the crater and the 60^{th} percentile of elevation values on the circle edge.

The calibration from HiRISE help us to constrain the error of the depth value extracted by our algorithm on CTX stereo-images. The error follows a Laplacian law with a standard deviation of about 5 m. We therefore, recommend using this pipeline to measure crater depth for crater larger than 100 m on CTX images.

HiRISE calibration shows that minimum elevation value within a crater must be avoided to estimate crater floor elevation, probably linked with local elevation anomalies or DEM errors.

We provide a python code that reproduce our pipeline. With this program and the MarsSI application, it becomes easy to compute large dataset of crater depth. This method may be extended to other datasets, as long as a crater shapefile is associated with a DEM. In this case, supplementary work should be done to assess errors on the measurements.

With about 17% of global coverage by CTX DEM, the algorithm offers large perspective to widely analyze the depth distribution of Martian craters down to 100 m. Such large depth dataset should help to better understand to interaction between surfaces processes and cratering mechanisms based on their shape distribution.

Acknowledgments

The research leading to these results has received funding from the European Research Council under the European Union's Seventh Framework Program (FP7/2007-2013)/ERC Grant agreement n° 280168. This paper has received the advice of Stuart Robbin and Gregory Michael.

Appendix A. Supplementary data

Supplementary material related to this article can be found, in the online version, at doi:https://doi.org/10.1016/j.mex.2019.08.007.

References

[1] M.H. Carr, J.W. Head, Geologic history of Mars, Earth Planet. Sci. Lett. 294 (2010) 185–203, doi:http://dx.doi.org/10.1016/j.epsl.2009.06.042.
[2] C.R. Chapman, Cratering on Mars I. Cratering and obliteration history, Icarus 22 (1974) 272–291, doi:http://dx.doi.org/10.1016/0019-1035(74)90177-8.
[3] H.J. Melosh, Impact Cratering: A Geologic Process, (1989).
[4] D.E. Wilhelms, The geologic history of the Moon, U.S. Geol. Surv. Prof. Pap. 1348 (1987) 302, doi:http://dx.doi.org/10.1007/s13398-014-0173-7.2.
[5] W.K. Hartmann, G. Neukum, Cratering chronology and the evolution of Mars, Space Sci. Rev. 96 (2001) 165–194, doi:http://dx.doi.org/10.1023/A:1011945222010.
[6] G.G. Michael, G. Neukum, Planetary surface dating from crater size–frequency distribution measurements: partial resurfacing events and statistical age uncertainty, Earth Planet. Sci. Lett. 294 (2010) 223–229, doi:http://dx.doi.org/10.1016/j.epsl.2009.12.041.
[7] G. Neukum, B.A. Ivanov, W.K. Hartmann, Cratering records in the inner solar system in relation to the lunar reference system, Space Sci. Rev. 96 (2001) 55–86, doi:http://dx.doi.org/10.1023/A:1011989004263.
[8] D. Stöffler, G. Ryder, Stratigraphy and isotope ages of lunar geologics units: chronological standard for the inner Solar System, Space Sci. Rev. (2001) 9–54.
[9] W.K. Hartmann, Martian cratering III: theory of crater obliteration, Icarus 15 (1971) 410–428, doi:http://dx.doi.org/10.1016/0019-1035(71)90119-9.
[10] G.G. Michael, Planetary surface dating from crater size–frequency distribution measurements: multiple resurfacing episodes and differential isochron fitting, Icarus 226 (2013) 885–890, doi:http://dx.doi.org/10.1016/j.icarus.2013.07.004.
[11] G.G. Michael, T. Kneissl, A. Neesemann, Planetary surface dating from crater size-frequency distribution measurements: Poisson timing analysis, Icarus 277 (2016) 279–285, doi:http://dx.doi.org/10.1016/j.icarus.2016.05.019.
[12] C. Quantin-Nataf, R.A. Craddock, F. Dubuffet, L. Lozac'h, M. Martinot, Decline of crater obliteration rates during early martian history, Icarus 317 (2019) 427–433, doi:http://dx.doi.org/10.1016/j.icarus.2018.08.005.
[13] E.S. Kite, J. Williams, A. Lucas, O. Aharonson, Constraints on early Mars atmospheric pressure inferred from small ancient craters, Astrophys. Astron. (2013) 1–27.
[14] E. Martellato, V. Vivaldi, M. Massironi, G. Cremonese, F. Marzari, A. Ninfo, J. Haruyama, Is the Linné impact crater morphology influenced by the rheological layering on the Moon's surface? Insights from numerical modeling, Meteorit. Planet. Sci. 52 (2017) 1388–1411, doi:http://dx.doi.org/10.1111/maps.12892.
[15] P.J. Mouginis-Mark, Martian fluidized crater morphology: variations with crater size, latitude, altitude, and target material, J. Geophys. Res. 84 (1979) 8011–8022.
[16] W.A. Watters, L.M. Geiger, M. Fendrock, R. Gibson, C.B. Hundal, The role of strength defects in shaping impact crater planforms, Icarus 286 (2017) 15–34, doi:http://dx.doi.org/10.1016/j.icarus.2016.12.024.
[17] N. Krishna, P.S. Kumar, Impact spallation processes on the Moon: a case study from the size and shape analysis of ejecta boulders and secondary craters of Censorinus crater, Icarus 264 (2016) 274–299, doi:http://dx.doi.org/10.1016/j.icarus.2015.09.033.
[18] L.L. Tornabene, W.A. Watters, G.R. Osinski, J.M. Boyce, T.N. Harrison, V. Ling, A.S. McEwen, A depth versus diameter scaling relationship for the best-preserved melt-bearing complex craters on Mars, Icarus 299 (2018) 68–83, doi:http://dx.doi.org/10.1016/j.icarus.2017.07.003.
[19] A.E. Williams, M.A. Persechino, The effect of projectile properties on target cratering, Int. J. Impact Eng. 5 (1987) 709–728.

[20] N. Mangold, S. Adeli, S. Conway, V. Ansan, B. Langlais, A chronology of early Mars climatic evolution from impact crater degradation, J. Geophys. Res. E: Planets 117 (2012) 1–22, doi:http://dx.doi.org/10.1029/2011JE004005.
[21] C.I. Fassett, B.J. Thomson, Crater degradation on the lunar maria: topographic diffusion and the rate of erosion on the Moon, J. Geophys. Res. Planets (2014) 1–17, doi:http://dx.doi.org/10.1002/2014JE004698.Received.
[22] J.W. Head, Processes of Lunar Crater degradation: changes in style with Geologic Time, Moon 12 (1975) 299–329, doi:http://dx.doi.org/10.1007/BF02629699.
[23] T. De Haas, E. Hauber, M.G. Kleinhans, Local late Amazonian boulder breakdown and denudation rate on Mars, Geophys. Res. Lett. 40 (2013) 3527–3531, doi:http://dx.doi.org/10.1002/grl.50726.
[24] J.B. Garvin, J.J. Frawley, Geometric properties of Martian impact craters: preliminary results from the mars orbiter laser altimeter, Geophys. Res. Lett. 25 (1998) 4405–4408, doi:http://dx.doi.org/10.1029/1998GL900177.
[25] M.P. Golombek, J.A. Grant, L.S. Crumpler, R. Greeley, R.E. Arvidson, J.F. Bell, C.M. Weitz, R.J. Sullivan, P.R. Christensen, L.A. Soderblom, S.W. Squyres, Erosion rates at the Mars Exploration Rover landing sites and long-term climate change on Mars, J. Geophys. Res. E: Planets 111 (2006) 1–14, doi:http://dx.doi.org/10.1029/2006JE002754.
[26] A.S. McEwen, B.S. Preblich, E.P. Turtle, N.A. Artemieva, M.P. Golombek, M. Hurst, R.L. Kirk, D.M. Burr, P.R. Christensen, The rayed crater Zunil and interpretations of small impact craters on Mars, Icarus 176 (2005) 351–381, doi:http://dx.doi.org/10.1016/j.icarus.2005.02.009.
[27] S.J. Robbins, B.M. Hynek, A new global database of Mars impact craters $\geq$1 km: 1. Database creation, properties, and parameters, J. Geophys. Res. E: Planets 117 (2012) 1–18, doi:http://dx.doi.org/10.1029/2011JE003966.
[28] T.F. Stepinski, M.P. Mendenhall, B.D. Bue, Machine cataloging of impact craters on Mars, Icarus 203 (2009) 77–87, doi:http://dx.doi.org/10.1016/j.icarus.2009.04.026.
[29] N. Warner, S. Gupta, S.Y. Lin, J.R. Kim, J.P. Muller, J. Morley, Late Noachian to Hesperian climate change on Mars: evidence of episodic warming from transient crater lakes near Ares Vallis, J. Geophys. Res. Planets 115 (2010), doi:http://dx.doi.org/10.1029/2009JE003522.
[30] W.A. Watters, L.M. Geiger, M. Fendrock, R. Gibson, Morphometry of small recent impact craters on Mars: size and terrain dependence, short-term modification, J. Geophys. Res. Planets 120 (2015) 226–254, doi:http://dx.doi.org/10.1002/2014JE004630.
[31] C.A. Wood, L. Andersson, New morphometric data for fresh lunar craters, Lunar Planet. Sci. Conf. 9th, Houston, Tex., 1978.
[32] N.K. Forsberg-Taylor, A.D. Howard, R.A. Craddock, Crater degradation in the Martian highlands: morphometric analysis of the Sinus Sabaeus region and simulation modeling suggest fluvial processes, J. Geophys. Res. 109 (2004) E05002, doi:http://dx.doi.org/10.1029/2004JE002242.
[33] S.J. Robbins, W.A. Watters, J.E. Chappelow, V.J. Bray, I.J. Daubar, R.A. Craddock, R.A. Beyer, M. Landis, L.R. Ostrach, L.L. Tornabene, J.D. Riggs, B.P. Weaver, Measuring impact crater depth throughout the solar system, Meteorit. Planet. Sci. 53 (2018) 583–637, doi:http://dx.doi.org/10.1111/maps.12956.
[34] R.A. Craddock, T.A. Maxwell, Geomorphic evolution of the Martian highlands through ancient fluvial processes, J. Geophys. Res. Planets 98 (1993) 3453–3468, doi:http://dx.doi.org/10.1029/92JE02508.
[35] Y. Matsubara, R.P. Irwin, R.A. Craddock, A.D. Howard, L. Bandeira, Impact crater depth and diameter changes on Noachian Mars, Lunar Planet. Sci. Conf. 48 (2017) 2818.
[36] C. Quantin-Nataf, O. Popova, W.K. Hartmann, S.C. Werner, Young Martian crater Gratteri and its secondary craters, J. Geophys. Res. Planets 121 (2016) 1118–1140, doi:http://dx.doi.org/10.1002/2015JE004864.
[37] C. Quantin-Nataf, L. Lozac'h, P. Thollot, D. Loizeau, B. Bultel, J. Fernando, P. Allemand, F. Dubuffet, F. Poulet, A. Ody, H. Clenet, C. Leyrat, S. Harrisson, MarsSI: Martian surface data processing information system, Planet. Space Sci. 150 (2018) 157–170, doi:http://dx.doi.org/10.1016/j.pss.2017.09.014.
[38] E. Smith, M.T. Zuber, V. Frey, J.B. Garvin, O. Muhleman, H. Pettengill, R.J. Phillips, H.J. Zwally, C. Duxbury, G. Lemoine, A. Neumann, D.D. Rowlands, O. Aharonson, P.G. Ford, A.B. Iranov, L. Johnson, J. Mcgovern, J.B. Abshire, R.S. Afzal, X. Sun, Mars Orbiter Laser Altimeter: experiment summary after the first year of global mapping of Mars, J. Geophys. Res. Atmos. 106 (2001) 689–722.
[39] K. Gwinner, R. Jaumann, E. Hauber, H. Hoffmann, C. Heipke, J. Oberst, G. Neukum, V. Ansan, J. Bostelmann, A. Dumke, S. Elgner, G. Erkeling, F. Fueten, H. Hiesinger, N.M. Hoekzema, E. Kersten, D. Loizeau, K.D. Matz, P.C. McGuire, V. Mertens, G.G. Michael, A. Pasewaldt, P. Pinet, F. Preusker, D. Reiss, T. Roatsch, R. Schmidt, F. Scholten, M. Spiegel, R. Stesky, D. Tirsch, S. Van Gasselt, S.H.G. Walter, M. Wählisch, K. Willner, The High Resolution Stereo Camera (HRSC) of Mars express and its approach to science analysis and mapping for Mars and its satellites, Planet. Space Sci. 126 (2016) 93–138, doi:http://dx.doi.org/10.1016/j.pss.2016.02.014.
[40] C. Heipke, J. Oberst, J. Albertz, M. Attwenger, P. Dorninger, E. Dorrer, M. Ewe, J.R. Kim, R.L. Kirk, H. Mayer, J.P. Muller, R. Rengarajan, M. Rentsch, R. Schmidt, F. Scholten, J. Shan, M. Spiegel, M. Wa, Evaluating planetary digital terrain models—the HRSC DTM test, Planet. Space Sci. 55 (2007) 2173–2191, doi:http://dx.doi.org/10.1016/j.pss.2007.07.006.
[41] J.R. Kim, J.P. Muller, Very high resolution stereo DTM extraction and its application to surface roughness estimation over Martian surface, Int. Arch. Photogramm. Remote Sens. Spat. Inf. Sci. 37 (2008) 993–998.
[42] M.C. Malin, J.F. Bell, B.A. Cantor, M.A. Caplinger, W.M. Calvin, R.T. Clancy, K.S. Edgett, L. Edwards, R.M. Haberle, P.B. James, S.W. Lee, M.A. Ravine, P.C. Thomas, M.J. Wolff, Context camera investigation on board the mars reconnaissance orbiter, J. Geophys. Res. 112 (2007) 1–25, doi:http://dx.doi.org/10.1029/2006JE002808.
[43] R.L. Kirk, E. Howington-Kraus, M.R. Rosiek, J.A. Anderson, B.A. Archinal, K.J. Becker, D.A. Cook, D.M. Galuszka, P.E. Geissler, T.M. Hare, I.M. Holmberg, L.P. Keszthelyi, B.L. Redding, W.A. Delamere, D. Gallagher, J.D. Chapel, E.M. Eliason, R. King, A.S. McEwen, Ultrahigh resolution topographic mapping of Mars with MRO HiRISE stereo images: meter-scale slopes of candidate Phoenix landing sites, J. Geophys. Res. Planets 114 (2009) 1–31, doi:http://dx.doi.org/10.1029/2007JE003000.
[44] A.S. Mcewen, E.M. Eliason, J.W. Bergstrom, N.T. Bridges, C.J. Hansen, W.A. Delamere, J.A. Grant, V.C. Gulick, K.E. Herkenhoff, L.P. Keszthelyi, R.L. Kirk, M.T. Mellon, S.W. Squyres, N. Thomas, C.M. Weitz, Mars reconnaissance orbiter's High Resolution Imaging Science Experiment (HiRISE), J. Geophys. Res. 112 (2007) 1–40, doi:http://dx.doi.org/10.1029/2005JE002605.
[45] D.E. Shean, O. Alexandrov, Z.M. Moratto, B.E. Smith, I.R. Joughin, C. Porter, P. Morin, An automated, open-source pipeline for mass production of digital elevation models (DEMs) from very-high-resolution commercial stereo satellite imagery, ISPRS J. Photogramm. Remote Sens. 116 (2016) 101–117, doi:http://dx.doi.org/10.1016/j.isprsjprs.2016.03.012.

[46] P.J. Mouginis-Mark, J.M. Boyce, V.L. Sharpton, H. Garbeil, Determination of Mars crater geometric data: insights from high-resolution digital elevation models, Meteorit. Planet. Sci. 15 (2017) 1–15, doi:http://dx.doi.org/10.1111/maps.12895.
[47] S.J. Robbins, I. Antonenko, M.R. Kirchoff, C.R. Chapman, C.I. Fassett, R.R. Herrick, K.N. Singer, M. Zanetti, C. Lehan, D. Huang, P.L. Gay, The variability of crater identification among expert and community crater analysts, Icarus 234 (2014) 109–131, doi:http://dx.doi.org/10.1016/j.icarus.2014.02.022.
[48] T. Kneissl, S. Van Gasselt, G. Neukum, Map-projection-independent crater size-frequency determination in GIS environments—new software tool for ArcGIS, Planet. Space Sci. 59 (2011) 1243–1254, doi:http://dx.doi.org/10.1016/j.pss.2010.03.015.
[49] J. Young, A statistical investigation of diameter and distribution of lunar craters, J. Br. Astron. Assoc. 50 (1940) 309–326.